Silica Particles Trigger Pulmonary Fibrosis Act Through Cell-To-Cell Delivery of Exosomal Mir-107

Di Wang
Zhengzhou University
Changfu Hao
Zhengzhou University
Wei Guo
Henan Institute for Occupational Medicine
Yangqing Pei
The First Affiliated Hospital of Zhengzhou University
Lin Zhang
Maternal and Child Health Care Hospital of Shandong Province
Lei Bao
Hebei Medical University
Suna Liu
Third Affiliated Hospital of Zhengzhou University
Yiping Li
Zhengzhou University
Yaqian Qu
Zhengzhou University
Youliang Zhao
Zhengzhou University
Mingcui Ding
Zhengzhou University
Wu Yao (yaowu@zzu.edu.cn)
Zhengzhou University https://orcid.org/0000-0001-7792-2714

Research

Keywords: Silica particles, Fibroblast, Transdifferentiation, Exosomes, miR-107

Posted Date: March 30th, 2021

DOI: https://doi.org/10.21203/rs.3.rs-365315/v1

Abstract

Background: Long-term exposure to inhalable silica particles may lead to a serious systemic pulmonary disease called silicosis. However, the role and mechanisms of exosomes in silicosis are not well understood. We previously reported that serum exosomal micro (mi) RNA profile was altered in pneumoconiosis patients and silica-exposed macrophages.This study was aimed to explore and verify the role of the exosomal miRNA in lung fibrosis when exposed to silica particles.

Results: The RT-qPCR result revealed that the levels of the miR-107, miR-122-5p, miR-125a-5p, miR-126-5p, and miR-335-5p were elevated in serous exosomes of silicosis patients. A bioinformatics analysis predicted 5 potential interactions involving these miRNAs, with miR-107–cyclin-dependent kinase (CDK) 6 having the highest score. In a mouse model of silica particle-induced silicosis, miR-107 level in serum exosomes and lung tissue was increased during the development of fibrosis, while inhibition of miR-107 reduced pulmonary fibrosis. The number of exosomes secreted by macrophages exposed to silica particles was also increased and showed altered cargo composition, and showed a capacity to promote lung fibroblast transdifferentiation through a possible mechanism involving the delivery of miR-107 by macrophages to lung fibroblasts via exosomes, resulting in targeted inhibition of CDK6, reduced retinoblastoma protein phosphorylation, and inhibition of E2F1 and cell cycle progression.

Conclusion: In summary, exosomal miR-107 derived from macrophages exposed to silica particles were transferred to pulmonary fibroblasts to trigger their transdifferentiation by targeting CDK6 and arresting cell cycle. These findings provide insight into the pathogenesis of silicosis and potential targets for intervention.

Background

Silicon is the second abundant element in the earth crust, mainly in the form of silicate and silica, which is widely found in rocks, gravel, and dust [1, 2]. As one of prominent compound used in daily life, production and scientific research, silica exist ubiquitously in nature and human environments, so it may resulted in a variety of adverse health effect especially in industrious conditions. Silicosis, a serious systemic disease, is characterized by irreversible pulmonary fibrosis caused by inhaled crystalline quartz dust. While preventable, many workers are still affected by silicosis and experience a progressive and fatal disease course because of substandard production processes and inadequate personal protection measures. To date, there is no effective treatment for silicosis. Clarifying the pathologic mechanisms of silicosis at the cellular and molecular levels can provide a basis for the development of effective treatments.

In silicosis, myofibroblasts are the main effector cells mediating fibrogenesis, extracellular matrix deposition, and tissue remodeling. Factors that induce fibroblast transdifferentiation include signaling molecules such as interleukin (IL)-1, IL-10, and transforming growth factor (TGF)-β [3–5]; mechanical

factors such as mechanical tension and cell adhesion [6–9]; and extracellular matrix proteins such as fibronectin [10, 11].

Micro (mi) RNAs are a family of small noncoding RNAs that modulate gene expression by inhibiting mRNA translation or degrading target mRNAs [12]. These molecules are widely distributed in vivo. miRNAs circulating in various body fluids mainly exist in a free form or are bound by lipoprotein or encapsulated by vesicles including exosomes, which are vesicles with a diameter of 30–150 nm that are secreted by eukaryotic cells and play an important role in intercellular signal communication. Exosomes have certain advantages for miRNA targeting because of their heterogeneity [13, 14], specificity [15, 16] and stability [17].

miRNAs have been shown to be involved in the regulation of fibroblast transdifferentiation. For example, miR-21 [18] and miR-145 [19, 20] were shown to promote transdifferentiation in pulmonary fibrosis diseases, whereas miR-9-5p [21], miR-22, miR-27a, miR-29, miR-31 [22], miR-101 [23], miR-1343 [24], and let-7d have an inhibitory role. These miRNAs mostly function by modulating the expression of genes encoding components of the TGF-β signaling pathway. In our previous study, we determined, by high-throughput sequencing, that the serum exosome miRNA profile of patients with pneumoconiosis was altered compared to that of normal control subjects, alteration also existed in exosome miRNA profile of macrophages (RAW264.7 cells) with or without silica particles exposure [25, 26], suggesting that exosomal miRNAs contribute to the development of silicosis. However, the mechanisms by which this is achieved remain unclear.

To address this issue, we investigated the role of miRNAs in the development of silicosis using clinical specimens and mouse and cell-based models of silicosis. The results showed that miR-107 level was higher in serous exosomes of patients and mice with silicosis. Inhibiting miR-107 alleviated silica particle-induced fibrosis in mice. We also investigated the mechanism of action of miR-107—including potential targets—in lung fibroblast transdifferentiation in vitro. Our results provide mechanistic insight into the pathogenesis of silicosis that can aid in the development of effective treatments.

Methods

Patients

A total of 50 male patients with silicosis were recruited at Henan Hospital for Occupational Diseases from April 1 to August 31, 2018. All patients were diagnosed with silicosis according to diagnostic criteria for occupational pneumoconiosis (GBZ-70-2015) based on chest X-ray or digital radiography, epidemiologic investigation, and physical examination. Additionally, 50 healthy control subjects who had not been previously exposed to silica were recruited from the First Affiliated Hospital of Zhengzhou University. Individuals with active tuberculosis, malignant tumor, recent infection, or other disorders that could affect the blood were excluded. A 3 ml sample of venous blood was collected from each subject;

the collection tubes were placed vertically for 30 min, followed by centrifugation at 3000 rpm for 10 min to separate the serum.

Mouse model of silicosis

Male C57BL/6N mice (4–6 weeks old) were purchased from Beijing Vital River Laboratory Animal Technology Co. (Beijing, China) and maintained in a specific pathogen-free environment at the College of Public Health, Zhengzhou University. The mice were exposed to silica particles by intratracheal instillation to establish the silicosis model, or to saline as a control, and sacrificed on days 1, 7, 14, 28, and 56 after exposure for analyses. Peripheral blood and lung tissue samples were collected. Serum was obtained as described above.

In vivo miR-107 antagomir treatment

Mice were randomly divided into 4 groups and were cotreated with either miR-107 antagomir (10 mg/kg; GenePharma, Shanghai, China) or a negative control miRNA (miR-NC) and silica suspension via intratracheal instillation, and then injected via the tail vein with miR-107 antagomir or miR-NC (4 mg/kg, GenePharma) or saline, weekly, for the next 3 weeks. Mice exposed to saline only served as the control. On day 28, the mice were sacrificed and peripheral blood and lung tissue samples were collected.

In vitro silicosis model

RAW264.7 cells were seeded at 1×10^5/ml in cell culture dishes (100 mm, Wuxi NEST Biotechnology Co., Wuxi, China) and cultured in complete medium. The following day, the medium was aspirated and the cells were washed 3 times with phosphate-buffered saline (PBS). Serum-free medium containing micron-sized silica particles (100 μg/ml; Sigma-Aldrich) or PBS was added to the dishes for 48 h. For exosome treatment, NIH-3T3 cells were seeded at 0.75×10^4/ml in a 6-well plate with complete medium. The following day, the medium was replaced with free-serum medium as described above. Cells were incubated with exosomes (about 1 μg at the protein level) secreted from macrophages exposed to silica (SiO_2-exo) or without exposure (c-exo) for 2 days, with cells incubated with PBS serving as the control. For TGF-β treatment, NIH-3T3 cells were treated with mouse recombinant TGF-β (Absin, Shanghai, China) at concentrations of 0, 1, 2, and 5 ng/ml. For miRNA transfection, RAW264.7 cells were treated with miR-107 mimic or the negative control (mimic-NC; 50 nM) (GenePharma, Shanghai, China) to enhance the endogenous level of miR-107. Additionally, NIH-3T3 and MRC-5 cells were treated with miR-107 or mimic-NC (50 nM), or miR-107 inhibitor or the corresponding negative control (inhibitor-NC; 100 nM) (GenePharma). NIH-3T3 cells were transfected with cyclin-dependent kinase (CDK) 6 plasmid (10 nM) (GeneChem) using Lipofectamine 3000 (Thermo Fisher Scientific, Waltham, MA, USA). In the cell recovery experiment, NIH-3T3 cells were transfected with miR-107 inhibitor and CDK6 small interfering (si) RNA. The culture medium was harvested for exosome extraction and cells were harvested for protein and RNA isolation.

Exosome isolation and characterization

Exosomes were isolated from human serum samples by 5 different methods (Supplementary Materials) and from cell culture medium by ultracentrifugation. For the latter, the medium was centrifuged at 2000×*g* for 30 min to remove cells and debris. The supernatant was transferred to a new tube and centrifuged at 10,000×*g* for 45 min to remove large vesicles. The supernatant was passed through a 0.22-μm filter and centrifuged at 110,000×*g* for 120 min (70 Ti rotor, Optima L-100K; Beckman Coulter, Brea, CA, USA). The precipitate was resuspended in PBS and centrifuged at 110,000×*g* for 70 min to obtain exosomes. The concentration and diameter of the exosomes were determined by nanoparticle tracking analysis (NTA) using a ZetaView instrument (Particle Metrix, Inning am Ammersee, Germany). Briefly, the sample was diluted with PBS to achieve the optimal detectable concentration for the analysis software. The diluted solution was injected into the laser chamber for detection, image output, and data recording. For morphologic analysis by transmission electron microscopy (TEM), exosome-enriched isolates were added as drops to electron microscope grids and negatively stained with 1% uranyl oxalate. Images were captured with a transmission electron microscope (HT7700; Hitachi High-Tech, Tokyo, Japan).

Target gene prediction

MiRWalk (http://mirwalk.umm.uni-heidelberg.de/) was used to predict miRNA target genes. Briefly, in the miRDB, TargetScan, and miRTarBase databases linked by miRWalk, target genes in the human and mouse genomes were selected based on the criterion of a score > 0.90 in at least 2 of the databases.

Histology

Mouse lung tissue samples were fixed in 4% paraformaldehyde, embedded in paraffin, and cut into sections at a thickness of 6 μm that were stained with hematoxylin and eosin (H&E) to evaluate the inflammation and damage to alveolar structure, or with Masson's trichrome to visualize collagen deposition.

RNA isolation and quantitation

Exosomal miRNA was extracted using an miRNA extraction kit (DP503, Tiangen Biotech, Beijing, China). Briefly, after lysis with MZA buffer, chloroform was added to the samples for RNA extraction. The upper aqueous phase was thoroughly mixed with ethanol and transferred to a column, and miRNAs were purified using MRD buffer. Total RNA was extracted using TRIzol reagent (Thermo Fisher Scientific) and the quality was assessed using a Nanodrop 2000 spectrophotometer (Thermo Fisher Scientific).

RNA was reverse transcribed into cDNA using miRcute Plus miRNA qPCR Detection Kit (KR211; Tiangen Biotech) or PrimeScript RT Reagent Kit with gDNA Eraser (RR047A; Takara Bio, Otsu, Japan), and quantitated by quantitative real-time (qRT-)PCR using the SYBR Green Kit (Tiangen Biotech; FP411) or TB Green Premix Ex Taq II (Takara Bio; RR820A). Relative levels of miRNAs and mRNAs were normalized to U6 and glyceraldehyde 3-phosphate dehydrogenase (GAPDH). The primers used for PCR amplification of miRNA and mRNA were synthesized by Tiangen Biotech and Takara Bio, respectively. All of the steps were carried out according to the manufacturers' recommendations.

Western blot analysis

Exosomes, cells, and lung tissue samples were lysed using radio immunoprecipitation assay lysis buffer (Beijing Dingguo Changsheng Biotechnology Co, Beijing, China) and total protein was quantified with the BCA Protein Quantitation Kit (Boster Bio, Pleasanton, CA, USA; AR0146). Total protein in the lysates was adjusted to the same concentration and denatured by boiling. Proteins were separated by sodium dodecyl sulfate polyacrylamide gel electrophoresis using precast gels (Beijing Dingguo Changsheng Biotechnology Co) and electrophoretically transferred to a polyvinylidene fluoride membrane that was blocked with 5% nonfat dry milk in Tris-buffered saline/Tween-20 solution and probed with antibodies against programmed cell death 6-interacting protein (ALIX), tumor susceptibility gene (TSG)101, cluster of differentiation (CD)63, and fibronectin (all from Proteintech, Rosemont, IL, USA); α-smooth muscle actin (α-SMA) and phosphorylated retinoblastoma (pRb) (both from Cell Signaling Technology, Danvers, MA, USA); cyclin D1 and E2F1 (both from Wanleibio, Shenyang, China); CDK6 (ABclonal, Woburn, MA, USA); collagen Ⅰ (Boster Bio); and retinoblastoma (Rb)1 (Zen-Bio, Research Triangle, NC, USA). GAPDH (Cell Signaling Technology) was used as the loading control.

Exosome uptake assay

Exosomes were incubated for 20 min at 37℃ in the dark with the cell membrane dye DiO (10 μM) (Beyotime, Shanghai, China). To remove free dye, exosomes were subjected to another round of isolation. NIH-3T3 cells were incubated with the cell membrane dye DiI (10 μM) (Beyotime) for 20 min and washed 3 times with PBS. The labeled exosomes were cocultured with the cells for 4 h. The cells were then fixed with 4% paraformaldehyde and the nuclei were stained with 4',6-diamidino-2-phenylindole (DAPI) before visualization with a laser scanning confocal microscope (TSC SP-8, Leica, Germany).

miRNA in situ hybridization and immunofluorescence analysis

After baking, deparaffinization, repair, and prehybridization with 0.5% Triton X-100 in PBS, lung tissue sections were hybridized overnight at 37℃ with digoxigenin-labeled miR-107 probes in hybridization buffer. The sections were incubated overnight at 4℃ with anti-collagen Ⅰ antibody (Boster Bio) and nuclei were stained with DAPI. Signals were detected with a laser scanning confocal microscope.

Cell cycle assay

NIH-3T3 cells transfected with miR-107 inhibitor or inhibitor-NC were harvested and fixed overnight at 4℃ with 70% cold ethanol. After washing twice with PBS, the cells were resuspended in propidium iodide/RNase staining solution (Beyotime) followed by incubation for 30 min at room temperature. Cell cycle distribution was analyzed by flow cytometry (Accuri C6; BD Biosciences, Franklin Lakes, NJ, USA) and ModFit software (Verity Software House, Topsham, ME, USA).

Dual luciferase assay

The 3'-untranslated region (UTR) of the *CDK6* gene was cloned into the pSI-Check2 vector (Hanbio, Shanghai, China) to obtain the reporter vector for the dual luciferase assay. HEK-293T cells were seeded in a 96-well plate and allowed to attach overnight. Reporter constructs with a mutated or wild-type 3'-UTR

of the *CDK6* gene were cotransfected into the cells with miR-107 mimic or mimic-NC. After 48 h, luciferase activity was measured using a commercial kit (Promega, Madison, WI, USA).

Statistical analysis

Statistical analyses were performed using SPSS v21.0 software (SPSS Inc, Chicago, IL, USA). Data are expressed as mean ± standard deviation. All statistical tests were 2-sided, and the level of statistical significance was set at $\alpha = 0.05$.

Results

Serum exosomal levels of 5 miRNAs are elevated in patients with silicosis

There was no difference in mean age between silicosis patients and healthy control subjects (Table 1), and no difference in mean working age among patients at different stages of the disease (Table 2).

Table 1
Age distribution of silicosis patients and healthy control subjects

Group	*N*	Mean age ± SD, years	*t*	*P*
Silicosis	50	51.72 ± 5.720	1.442	0.152
Control	50	50.24 ± 4.470		

Table 2
Age and working age of silicosis patients at different stages of disease

Stage	*N*	Mean age ± SD, years	Mean working age ± SD, years
	24	51.88 ± 6.311	16.73 ± 10.334
	12	50.21 ± 5.046	17.67 ± 9.851
	14	52.21 ± 5.533	16.67 ± 6.832
F		0.198	0.048
P		0.821	0.953

In our previous study, we isolated exosomes from the serum of pneumoconiosis patients, healthy controls, and from macrophages with or without exposure to silica for high-throughput miRNA sequencing. Bioinformatics analysis identified 7 miRNAs that were differentially expressed: miR-27b-5p, miR-30c-2-3p, miR-107, miR-122-5p, miR-125a-5p, miR-126-5p, and miR-335-5p [26]. The differential

expression of miR-107, miR-122-5p, miR-125a-5p, miR-126-5p, and miR-335-5p in was confirmed by qRT-PCR (Fig. 1a). To determine whether the expression of these 5 miRNAs changed over the course of the disease, we compared their levels in serous exosomes of patients at different stages of silicosis and found that they were lower at stage II than at stage I, while miR-122-5p and miR-335-5p levels were higher at stage □ than at stage □ (Fig. 1b).

Target gene prediction

Potential target genes of the 5 differentially expressed miRNAs were predicted with miRWalk. The prediction algorithm identified 293 genes in humans potentially regulated by hsa-miR-107, 119 by hsa-miR-122-5p, 371 by hsa-miR-125a-5p, 3 by hsa-miR-126a-5p, and 21 by hsa-miR-335-5p. Additionally, 2 putative target genes of mmu-miR-107, 8 of mmu-miR-122-5p, 9 of mmu-miR-125a-5p, and 4 of mmu-miR-126a-5p were identified in mice. Five potential interactions were identified using Venn 2.1.0: miR-107–CDK6, miR-122-5p–transcription factor (TF) DP2, miR-125a-5p–tumor necrosis factor receptor-associated factor 6, miR-125a-5p–chromobox homolog (CBX)7, and miR-125a-5p–V-set immunoregulatory receptor (VSIR) (Fig. 1c), with miR-107–CDK6 having the highest prediction score.

Temporal profile of miR-107 in serum exosomes and lung tissue of mice

Inflammatory cell infiltration was observed on day 1 after silica instillation by H&E staining. The alveolar wall was thickened and alveolar structure disrupted by day 7, while inflammatory cell accumulation and cell nodules were observed on day 28. By day 56, the alveolar structure was completely destroyed and collagen deposition was markedly increased, as visualized by Masson's trichrome staining (Fig. 2a,b). These histologic changes were accompanied by the gradual increase in expression of the fibrosis markers α-SMA, collagen □, and fibronectin in lung tissue and decrease in that of CDK6 (Fig. 2c).

The temporal profile of miR-107 expression in serous exosomes and lung tissue was evaluated by qRT-PCR. miR-107 level in serous exosomes was decreased relative to the control group on day 7 after silica exposure but increased gradually starting from day 14 (Fig. 2d). Similarly, miR-107 level in lung tissue was decreased on day 7 but increased gradually starting from day 28 (Fig. 2e). Pearson correlation analysis revealed a positive correlation between miR-107 levels in serum exosomes and lung tissue ($r = 0.834$, $P < 0.001$).

Inhibition of miR-107 alleviates silica-induced pulmonary fibrosis in vivo

To investigate the effect of miR-107 on silica-induced pulmonary fibrosis in mice, we inhibited miR-107 with an antagomir. miR-107 level was markedly reduced in silicosis mice treated with the antagomir as determined by qRT-PCR, indicating that the inhibition was successful (Fig. 3b). H&E and Masson's trichrome staining showed that this resulted in the disappearance of the large cell nodules and collagen

accumulation observed in silica-exposed mice with antagomir treatment (Fig. 3c). Additionally, western blot analysis revealed that the expression of fibrosis markers was downregulated whereas that of CDK6 was upregulated (Fig. 3d); and in situ hybridization and immunofluorescence analyses demonstrated that miR-107 and collagen Ⅰ levels were reduced (Fig. 3e). These results indicate that miR-107 antagomir attenuates silica-induced pulmonary fibrosis.

Characterization of exosomes derived from macrophages

Particles isolated from the culture medium of RAW264.7 cells were analyzed by TEM. We observed the cup-shaped vesicles that have been described in other studies [27] (Fig. 4a). NTA showed that although particle size was unaffected, silica treatment increased their concentration (Fig. 4b-d). Western blot analysis revealed that the isolated particles were positive for the exosome markers CD9, CD81, and TSG101, which were upregulated after exposure to silica (Fig. 4e). These results suggest that silica exposure enhances exosome secretion from RAW264.7 cells.

miR-107 levels are elevated in silica-exposed macrophages, their secretory exosomes, and effector cells

To examine the uptake of exosomes, the fluorescent lipophilic dyes DiO and DiI were used to stain exosomes and fibroblasts, respectively. After 4 h, NIH-3T3 cells were spindle-shaped and punctate exosomes surrounded the cells or were fused to the cell membrane. There were no significant differences in exosome number and distribution between cells with and those without exposure to silica, suggesting comparable uptake of exosomes (Fig. 5a). We examined miR-107 expression in macrophages, their secreted exosomes, and NIH-3T3 cells treated with exosomes and found that the levels in macrophages (Fig. 5b) and exosomes (Fig. 5c) were increased following silica exposure. Notably, miR-107 level was also increased in NIH-3T3 cells incubated with exosomes derived from macrophages exposed to silica particles (SiO_2-exo) (Fig. 5d).

Exosomes derived from silica-exposed macrophages promote transdifferentiation of pulmonary fibroblasts

To evaluate the effect of exosomes on fibroblast effector cells, exosomes derived from macrophages were incubated with NIH-3T3 cells. Western blot analysis indicated that SiO_2-exo, but not c-exo, increased the expression of the differentiation markers α-SMA, collagen Ⅰ, and fibronectin (Fig. 5e). To determine whether miR-107 encapsulated in exosomes can promote fibroblast transdifferentiation, we transfected macrophages with synthetic miR-107 or mimic-NC. As expected, exosomal miR-107 level was increased (Fig. 5f), which was accompanied by enhanced NIH-3T3 cell transdifferentiation and downregulation of CDK6 (Fig. 5g).

miR-107 potentiates the profibrogenic effect of TGF-β in vitro

To determine whether CDK6 is a target of miR-107 inhibition, we first predicted the potential binding sites of the miR-107 seed sequence in the human and mouse *CDK6* 3'-UTR using TargetScan (Fig. 6a). The results of the dual-luciferase reporter assay showed that miR-107 mimic decreased luciferase activity in cells transfected with the wild-type *CDK6* 3'-UTR sequence but not in those transfected with the mutated sequence (Fig. 6b), suggesting that *CDK6* is directly regulated by miR-107. A search of the Kyoto Encyclopedia of Genes and Genomes databases showed that CDK6 is involved in cell cycle-associated signaling downstream of TGF-β; we therefore treated NIH-3T3 cells with different concentrations of TGF-β and found that at 2 ng/ml, miR-107 was upregulated whereas CDK6 was downregulated (Fig. 6c, d), and used this concentration in subsequent experiments.

To evaluate the effect of miR-107 on fibroblast transdifferentiation, NIH-3T3 cells were transfected with miR-107 mimic. miR-107 expression was 1000 times higher in these cells compared to control cells (Fig. 6e), and fibroblast differentiation markers were upregulated whereas *CDK6* was downregulated (Fig. 6f, g). The opposite effect was observed upon transfection of miR-107 inhibitor (Fig. 6h–j). The same results were obtained using MRC-5 human embryo lung fibroblasts (Fig. S2).

To further confirm the effect of CDK6 on fibroblast transdifferentiation, NIH-3T3 cells were transfected with CDK6 overexpression plasmid, which resulted in decreased expression of differentiation markers (Fig. 7a). We also performed a cell recovery experiment by transfecting cells with *CDK6* siRNA, with cells transfected with *GAPDH* siRNA serving as a positive control (Fig. 7b). Of the 3 *CDK6* siRNAs that were tested, siRNA-2 had the highest knockdown efficiency (Fig. 7c). Cotransfection of *CDK6* siRNA abrogated the antifibrotic effect of miR-107 inhibitor (Fig. 7d).

miR-107 modulates fibroblast transdifferentiation by targetingCDK6

As CDK6 is involved in cell cycle regulation, we transfected NIH-3T3 cells with miR-107 inhibitor and analyzed cell cycle distribution by flow cytometry. Inhibition of miR-107 reduced the size of the G1 fraction and increased the proportion of cells in S phase (Fig. 7e); moreover, it increased the expression of proteins involved in cell cycle signaling including cyclin D, pRb, and E2F1 (Fig. 7f).

Discussion

Long-term silica particle inhalation leads to silicosis. Myofibroblasts are terminal effector cells in the development of pulmonary fibrosis, and the activation and transdifferentiation of pulmonary fibroblasts is critical for this process. Given that exosomes mediate intercellular signaling in various physiologic and pathologic contexts, the present study examined the role of exosomal miR-107 in the pathogenesis of silicosis. Our results showed that miR-107 levels in lung tissue and serum exosomes increased following inflammation induced by exposure to silica, while inhibition of miR-107 attenuated pulmonary fibrosis. Exosomal miR-107 derived from silica particle-exposed macrophages promoted the transdifferentiation of lung fibroblasts, possibly through targeted inhibition of CDK6, pRb, and E2F1.

Exosomes are widely distributed in body fluids and can carry nucleic acids, proteins, and lipids, among other biomolecules. These vesicles are internalized by other cells via direct membrane fusion, endocytosis, or cell type-specific phagocytosis to exert biological effects[28]. Exosomal miRNAs are known to regulate gene expression. The species of exosomal miRNAs in tissue or body fluids varies for different diseases [29–31]. We found that the levels of miR-107, miR-122-5p, miR-125a-5p, miR-126-5p, and miR-335-5p were higher in serous exosomes of silicosis patients than in those of healthy control subjects, suggesting that these 5 miRNAs can serve as diagnostic biomarkers or potential therapeutic targets in the treatment of silicosis. The lower levels of these miRNAs in stage Ⅱ as compared to stage I or III patients may be due to the small number of subjects in our study.

We focused on the miR-107–CDK6 interaction in the present study. miR-107 has been implicated in cell cycle regulation in various physiologic as well as pathologic processes such as Alzheimer disease, cancer, and diabetes. For example, miR-107 expression was found to decrease with age, and is thought to play an important role in regulating biological life span[32]. As a tumor suppressor, miR-107 negatively regulates cell proliferation, migration, and apoptosis, and was shown to inhibit the proliferation and migration of breast cancer cells by targeting CDK8r[33]. miR-107 is downregulated in patients with osteoarthritis and its upregulation enhanced aggrecan and collagen II protein expression in chondrocytes while reducing that of matrix metalloproteinase (MMP)13 and MMP9[34]. However, there have been few studies on the role of miR-107 in fibrotic diseases. Patients with cystic fibrosis showed increased levels of miR-103a-3p, miR-103b, and miR-107[35], but miR-107 was downregulated in chronic graft dysfunction with interstitial fibrosis and tubular atrophy following renal transplantation [36]. In our study, miR-107 levels in serous exosomes of silicosis patients and mouse lung tissue were decreased during inflammation and increased during fibrosis. Silica particle treatment also increased miR-107 level in macrophages along with their secreted exosomes and effector cells (fibroblasts). Overexpression of miR-107 promoted transdifferentiation of RAW264.7 cells and fibroblasts, whereas miR-107 inhibition had the opposite effect and alleviated silica particle-induced fibrosis in mice. Thus, miR-107 functions as a regulator of fibroblast transdifferentiation during fibrosis.

CDK6 is involved in cell cycle progression and cell differentiation. In eukaryotes, G1 arrest is a prerequisite for cell differentiation[37]. Overexpression of CDK6 was shown to inhibit the differentiation of glial precursor cells into astrocytes [38] and suppress BMP-2–induced osteoblast differentiation[39]. In the present study, we observed an inverse relationship between CDK6 and miR-107 expression, and confirmed the negative regulatory relationship with the dual luciferase reporter assay. We also found that the expression of transdifferentiation markers in fibroblasts was negatively regulated by CDK6; this may be related to cell cycle progression, given that inhibition of miR-107 promoted G1–S transition.

To further clarify the mechanism by which inhibition of CDK6 by miR-107 promotes silicosis, we examined the expression of the cell cycle signaling proteins cyclin D, pRb, Rb, and E2F1. Cyclins and CDKs synergistically promote Rb phosphorylation, leading to the dissociation of pRb and its binding partner E2F1; free E2F activates the transcription of DNA replication-related genes. Cyclin D is a regulator of CDK kinase, which forms a complex with CDK4 or CDK6 in which it functions as the regulatory subunit.

Cyclin D activity is necessary for the G1/S transition. Rb is a tumor suppressor that plays an important role in regulating cell cycle progression and DNA replication by binding E2F family transcription factors[40] as well as in the differentiation of eyes, lens, brain, nervous system, epidermis, melanocytes, hair cells, muscle, and liver[41]. Rb protein is the main G1 checkpoint for entry into S phase and cell growth, and promotes terminal differentiation by inducing cell cycle exit and tissue-specific gene expression[42]. It may also play a role in cell proliferation following differentiation[43]. E2F1 forms a heterodimer with TFDP2 to activate the transcription of cell cycle regulatory genes. In our study, inhibition of miR-107 increased the expression of cyclin D, pRb, and E2F1. Thus, in silicosis, the elevated levels of miR-107 in lung tissue and serum exosomes during silicosis may inhibit the expression of cyclin D and CDK6, leading to decreased phosphorylation of Rb and downregulation E2F1, which block cell cycle progression and promote the transcription of cell differentiation-related genes. However, proliferation and differentiation are not mutually exclusive; the former is essential for expanding the pool of cells that will undergo terminal differentiation, and cells in higher organisms cease to divide only at the end of this process.

Conclusion

In summary, inhibition of miR-107 reduced pulmonary fibrosis in a mouse model of silicosis. Exosomal miR-107 derived from macrophages exposed to silica particles promoted transdifferentiation of lung fibroblasts by inhibiting CDK6 and blocking cell cycle progression. These results highlight the role of exosomal miR-107 in the pathogenesis of silicosis and provide potential targets for its treatment.

Declarations

Acknowledgements

The authors thank the members of the Basic Medical College and Central Laboratory of School of Public Health, Zhengzhou University for their comments and suggestions, and the reviewers who made valuable suggestions that improved the quality of the presentation.

Funding

This work was also funded by the National Natural Science Foundation of China [81773404 and 81472954].

Availability of data and materials

The datasets during and/or analysed during the current study are available from the corresponding author on reasonable request.

Authors' contributions

DW designed, performed the experimental work and drafted the manuscript. WY, CH designed, supervised the study. YP, WG contributed to the silicosis analyses and their interpretation. LZ, LB, SL analyzed and interpreted the data. YL, QQ performed the experimental work and organize data. YZ, MD revised the manuscript. All authors read and approved the final manuscript.

Ethics approval

All study participants were informed about the study and provided signed consent. The experimental protocol was approved by the Ethics Committee of Zhengzhou University.

Consent for publication

No personal information is included in this study.

Competing interests

The authors declare that they have no competing interests.

References

1. Zhang X, Brodus D, Hollimon V, Hu H: A brief review of recent developments in the designs that prevent bio-fouling on silicon and silicon-based materials. Chem Cent J 2017, 11:18.
2. Leung CC, Yu IT, Chen W: Silicosis. Lancet 2012, 379(9830):2008-2018.
3. Hashimoto S, Gon Y, Takeshita I, Maruoka S, Horie T: IL-4 and IL-13 induce myofibroblastic phenotype of human lung fibroblasts through c-Jun NH2-terminal kinase-dependent pathway. J Allergy Clin Immunol 2001, 107(6):1001-1008.
4. Lei L, Zhao C, Qin F, He ZY, Wang X, Zhong XN: Th17 cells and IL-17 promote the skin and lung inflammation and fibrosis process in a bleomycin-induced murine model of systemic sclerosis. Clin Exp Rheumatol 2016, 34 Suppl 100(5):14-22.
5. Jagirdar J, Begin R, Dufresne A, Goswami S, Lee TC, Rom WN: Transforming growth factor-beta (TGF-beta) in silicosis. Am J Respir Crit Care Med 1996, 154(4 Pt 1):1076-1081.
6. Wang J, Chen H, Seth A, McCulloch CA: Mechanical force regulation of myofibroblast differentiation in cardiac fibroblasts. Am J Physiol Heart Circ Physiol 2003, 285(5):H1871-1881.
7. Hinz B: Mechanical aspects of lung fibrosis: a spotlight on the myofibroblast. Proc Am Thorac Soc 2012, 9(3):137-147.
8. Hinz B, Celetta G, Tomasek JJ, Gabbiani G, Chaponnier C: Alpha-smooth muscle actin expression upregulates fibroblast contractile activity. Mol Biol Cell 2001, 12(9):2730-2741.
9. Michalik M, Pierzchalska M, Wlodarczyk A, Wojcik KA, Czyz J, Sanak M, Madeja Z: Transition of asthmatic bronchial fibroblasts to myofibroblasts is inhibited by cell-cell contacts. Respir Med 2011, 105(10):1467-1475.

10. Kohan M, Muro AF, Bader R, Berkman N: The extra domain A of fibronectin is essential for allergen-induced airway fibrosis and hyperresponsiveness in mice. J Allergy Clin Immunol 2011, 127(2):439-446 e431-435.
11. Nakahara H, Gabazza EC, Fujimoto H, Nishii Y, D'Alessandro-Gabazza CN, Bruno NE, Takagi T, Hayashi T, Maruyama J, Maruyama K et al: Deficiency of tenascin C attenuates allergen-induced bronchial asthma in the mouse. Eur J Immunol 2006, 36(12):3334-3345.
12. Liang Y, Zou Q, Yu W: Steering Against Wind: A New Network of NamiRNAs and Enhancers. Genomics Proteomics Bioinformatics 2017, 15(5):331-337.
13. Momen-Heravi F, Saha B, Kodys K, Catalano D, Satishchandran A, Szabo G: Increased number of circulating exosomes and their microRNA cargos are potential novel biomarkers in alcoholic hepatitis. J Transl Med 2015, 13:261.
14. Wang J, Yan F, Zhao Q, Zhan F, Wang R, Wang L, Zhang Y, Huang X: Circulating exosomal miR-125a-3p as a novel biomarker for early-stage colon cancer. Sci Rep 2017, 7(1):4150.
15. Perge P, Butz H, Pezzani R, Bancos I, Nagy Z, Paloczi K, Nyiro G, Decmann A, Pap E, Luconi M et al: Evaluation and diagnostic potential of circulating extracellular vesicle-associated microRNAs in adrenocortical tumors. Sci Rep 2017, 7(1):5474.
16. Ebrahimkhani S, Vafaee F, Young PE, Hur SSJ, Hawke S, Devenney E, Beadnall H, Barnett MH, Suter CM, Buckland ME: Exosomal microRNA signatures in multiple sclerosis reflect disease status. Sci Rep 2017, 7(1):14293.
17. Aqil F, Kausar H, Agrawal AK, Jeyabalan J, Kyakulaga AH, Munagala R, Gupta R: Exosomal formulation enhances therapeutic response of celastrol against lung cancer. Exp Mol Pathol 2016, 101(1):12-21.
18. Liu G, Friggeri A, Yang Y, Milosevic J, Ding Q, Thannickal VJ, Kaminski N, Abraham E: miR-21 mediates fibrogenic activation of pulmonary fibroblasts and lung fibrosis. J Exp Med 2010, 207(8):1589-1597.
19. Yang S, Cui H, Xie N, Icyuz M, Banerjee S, Antony VB, Abraham E, Thannickal VJ, Liu G: miR-145 regulates myofibroblast differentiation and lung fibrosis. FASEB J 2013, 27(6):2382-2391.
20. Megiorni F, Cialfi S, Cimino G, De Biase RV, Dominici C, Quattrucci S, Pizzuti A: Elevated levels of miR-145 correlate with SMAD3 down-regulation in cystic fibrosis patients. J Cyst Fibros 2013, 12(6):797-802.
21. Fierro-Fernandez M, Busnadiego O, Sandoval P, Espinosa-Diez C, Blanco-Ruiz E, Rodriguez M, Pian H, Ramos R, Lopez-Cabrera M, Garcia-Bermejo ML et al: miR-9-5p suppresses pro-fibrogenic transformation of fibroblasts and prevents organ fibrosis by targeting NOX4 and TGFBR2. EMBO Rep 2015, 16(10):1358-1377.
22. Yang S, Xie N, Cui H, Banerjee S, Abraham E, Thannickal VJ, Liu G: miR-31 is a negative regulator of fibrogenesis and pulmonary fibrosis. FASEB J 2012, 26(9):3790-3799.
23. Huang C, Xiao X, Yang Y, Mishra A, Liang Y, Zeng X, Yang X, Xu D, Blackburn MR, Henke CA et al: MicroRNA-101 attenuates pulmonary fibrosis by inhibiting fibroblast proliferation and activation. J

Biol Chem 2017, 292(40):16420-16439.

24. Stolzenburg LR, Wachtel S, Dang H, Harris A: miR-1343 attenuates pathways of fibrosis by targeting the TGF-beta receptors. Biochem J 2016, 473(3):245-256.
25. Zhang L, Hao C, Yao S, Tang R, Guo W, Cong H, Li J, Bao L, Wang D, Li Y et al: Exosomal miRNA Profiling to Identify Nanoparticle Phagocytic Mechanisms. Small 2018, 14(15):e1704008.
26. Wang D, Hao C, Zhang L, Zhang J, Liu S, Li Y, Qu Y, Zhao Y, Huang R, Wei J et al: Exosomal miR-125a-5p derived from silica-exposed macrophages induces fibroblast transdifferentiation. Ecotoxicol Environ Saf 2020, 192:110253.
27. Thery C, Amigorena S, Raposo G, Clayton A: Isolation and characterization of exosomes from cell culture supernatants and biological fluids. Curr Protoc Cell Biol 2006, Chapter 3:Unit 3 22.
28. Svensson KJ, Christianson HC, Wittrup A, Bourseau-Guilmain E, Lindqvist E, Svensson LM, Morgelin M, Belting M: Exosome uptake depends on ERK1/2-heat shock protein 27 signaling and lipid Raft-mediated endocytosis negatively regulated by caveolin-1. J Biol Chem 2013, 288(24):17713-17724.
29. Motawi TK, Mohamed MR, Shahin NN, Ali MAM, Azzam MA: Time-course expression profile and diagnostic potential of a miRNA panel in exosomes and total serum in acute liver injury. Int J Biochem Cell Biol 2018, 100:11-21.
30. Nedaeinia R, Manian M, Jazayeri MH, Ranjbar M, Salehi R, Sharifi M, Mohaghegh F, Goli M, Jahednia SH, Avan A et al: Circulating exosomes and exosomal microRNAs as biomarkers in gastrointestinal cancer. Cancer Gene Ther 2017, 24(2):48-56.
31. Kim S, Choi MC, Jeong JY, Hwang S, Jung SG, Joo WD, Park H, Song SH, Lee C, Kim TH et al: Serum exosomal miRNA-145 and miRNA-200c as promising biomarkers for preoperative diagnosis of ovarian carcinomas. J Cancer 2019, 10(9):1958-1967.
32. Noren Hooten N, Abdelmohsen K, Gorospe M, Ejiogu N, Zonderman AB, Evans MK: microRNA expression patterns reveal differential expression of target genes with age. PLoS One 2010, 5(5):e10724.
33. Li XY, Luo QF, Wei CK, Li DF, Li J, Fang L: MiRNA-107 inhibits proliferation and migration by targeting CDK8 in breast cancer. Int J Clin Exp Med 2014, 7(1):32-40.
34. Tian F, Wang J, Zhang Z, Yang J: miR-107 modulates chondrocyte proliferation, apoptosis, and extracellular matrix synthesis by targeting PTEN. Int J Clin Exp Pathol 2019, 12(2):488-497.
35. Ideozu JE, Zhang X, Rangaraj V, McColley S, Levy H: Microarray profiling identifies extracellular circulating miRNAs dysregulated in cystic fibrosis. Sci Rep 2019, 9(1):15483.
36. Scian MJ, Maluf DG, David KG, Archer KJ, Suh JL, Wolen AR, Mba MU, Massey HD, King AL, Gehr T et al: MicroRNA profiles in allograft tissues and paired urines associate with chronic allograft dysfunction with IF/TA. Am J Transplant 2011, 11(10):2110-2122.
37. Sherr CJ: G1 phase progression: cycling on cue. Cell 1994, 79(4):551-555.
38. Ericson KK, Krull D, Slomiany P, Grossel MJ: Expression of cyclin-dependent kinase 6, but not cyclin-dependent kinase 4, alters morphology of cultured mouse astrocytes. Mol Cancer Res 2003, 1(9):654-

664.

39. Ogasawara T, Kawaguchi H, Jinno S, Hoshi K, Itaka K, Takato T, Nakamura K, Okayama H: Bone morphogenetic protein 2-induced osteoblast differentiation requires Smad-mediated down-regulation of Cdk6. Mol Cell Biol 2004, 24(15):6560-6568.
40. Macaluso M, Montanari M, Cinti C, Giordano A: Modulation of cell cycle components by epigenetic and genetic events. Semin Oncol 2005, 32(5):452-457.
41. Ajioka I: Coordination of proliferation and neuronal differentiation by the retinoblastoma protein family. Dev Growth Differ 2014, 56(5):324-334.
42. Weinberg RA: The retinoblastoma protein and cell cycle control. Cell 1995, 81(3):323-330.
43. Sage C, Huang M, Karimi K, Gutierrez G, Vollrath MA, Zhang DS, Garcia-Anoveros J, Hinds PW, Corwin JT, Corey DP et al: Proliferation of functional hair cells in vivo in the absence of the retinoblastoma protein. Science 2005, 307(5712):1114-1118.

Figures

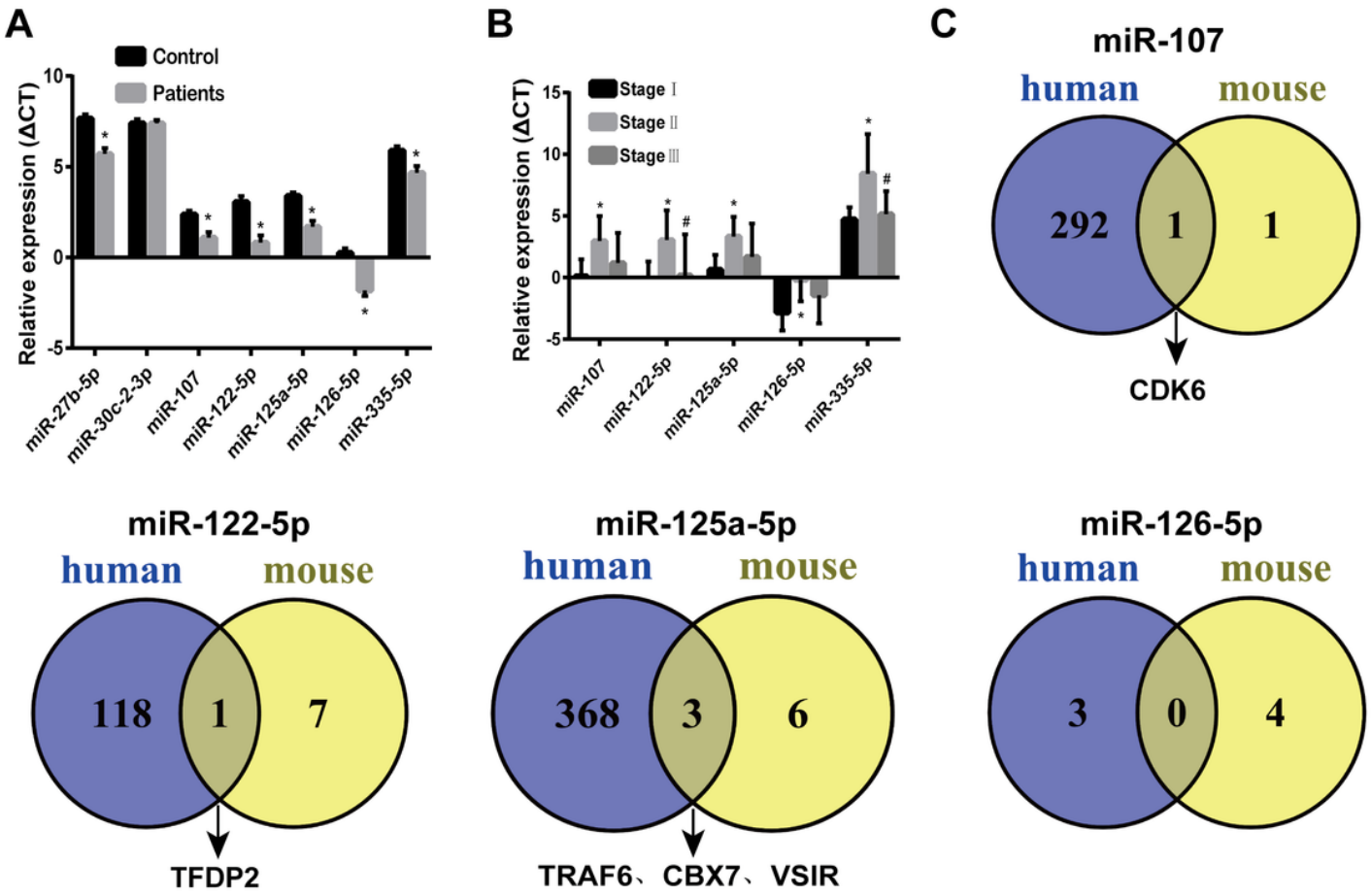

Figure 1

Differentially expressed miRNAs validation and target gene prediction. Relative levels of those seven miRNAs in serous exosomes of silicosis patients by RT-qPCR analysis (n=50) (a). U6 was used as an endogenous control. Error bars indicate mean ± standard deviation. * P<0.05. Relative levels of five miRNAs in serous exosomes from silicosis patients with different stages (n=50) (b). U6 was used as an endogenous control. Error bars indicate mean ± standard deviation. * Stage Ⅱ vs. Stage Ⅰ, # Stage Ⅲ vs. Stage Ⅱ, and P<0.05 for * and #. C, Venn diagram of target genes from human and mouse origin for miR-107, miR-122-5p, miR-125a-5p, and miR-126-5p.

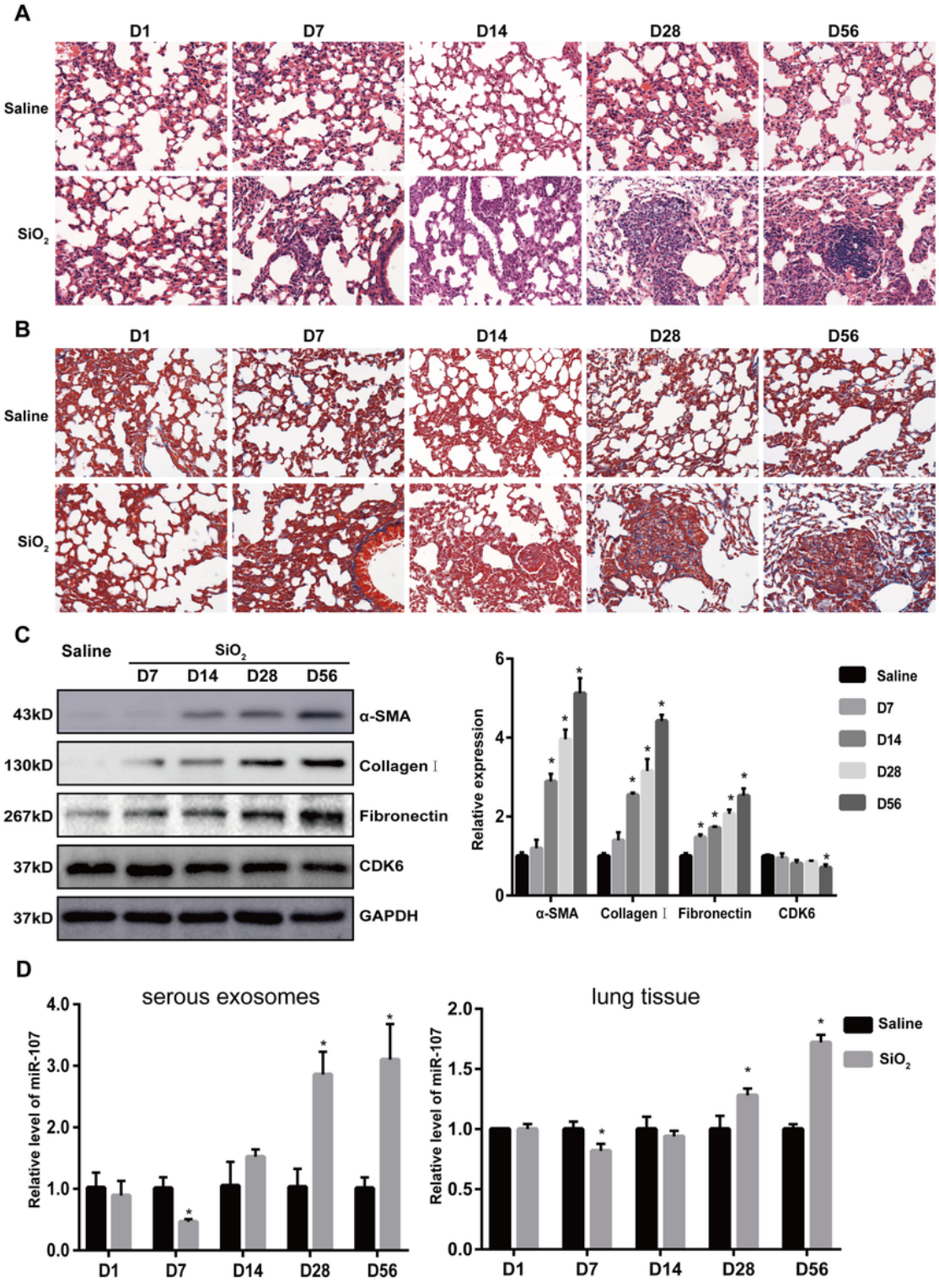

Figure 2

Validation of murine model of silicosis. Mice lung tissue sections were stained with hematoxylin and eosin (a) and Masson trichrome stainingafter (b) silica particles (50 μg/mL) or saline exposure for 1, 7, 14, 28, 56 days (200×). Expression of fibrosis markers (α-SMA, Collagen Ⅰ and Fibronectin) and CDK6 analyzed by Western blot (c). GAPDH was used as an endogenous control. The experiment were performed three times. *compared to saline, P<0.05. Relative levels of miR-107 in serous exosomes and lung tissue of mice (n=5) (d). *P<0.05. Error bars indicate mean ± standard deviation.

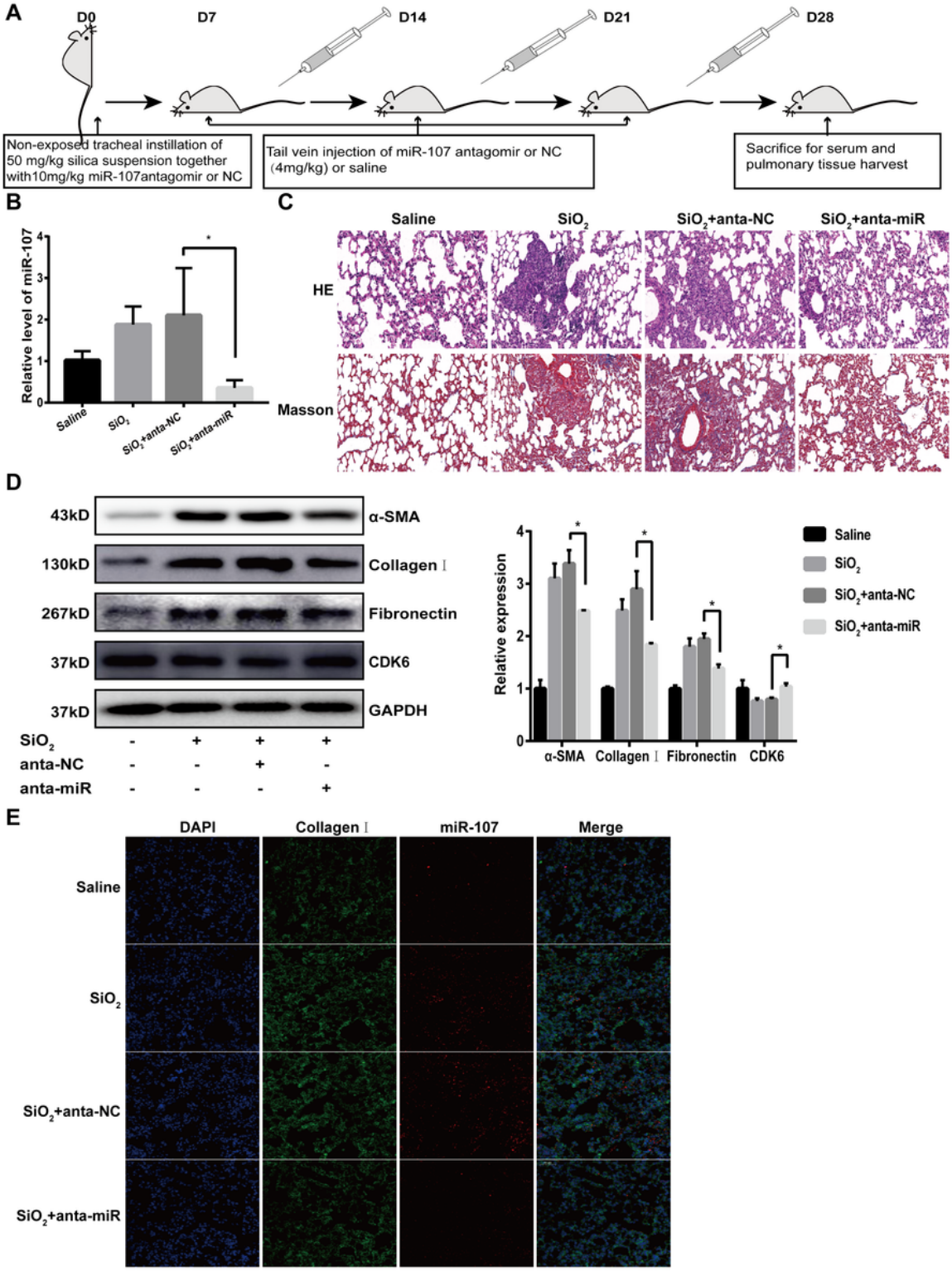

Figure 3

Intervention effect of miR-107 in silicosis mice. Sketch map of miR-107 intervention in silicosis mice (a). Relative levels of miR-107 in lung tissue of different groups (n=5) (b). Images of sections stained by hematoxylin and eosin and Masson trichrome staining (c). Expression of fibrosis markers and CDK6 analyzed by Western blot (d). GAPDH was used as an endogenous control. The experiment was performed three times. Collagen Ⅰ expression and miR-107 level of sections captured using a laser scanning confocal microscope (e). Saline, mice exposed to saline; SiO2, mice instilled with silica particles (50 mg/mL) via non-exposed tracheal following injected with saline via tail vein. SiO2+NC, mice instilled with silica particles (50 mg/kg) and antagomir negative control (10 mg/mL) via non-exposed tracheal following injected with antagomir negative control (4 mg/kg) via tail vein. SiO2+miR, mice instilled with silica particles (50 mg/kg) and antagomir miR-107 (10 mg/mL) via non-exposed tracheal following injected with antagomir miR-107 (4 mg/kg) via tail vein. *SiO2+anta-NC vs. SiO2+anta-miR, P<0.05. Error bars indicate mean ± standard deviation.

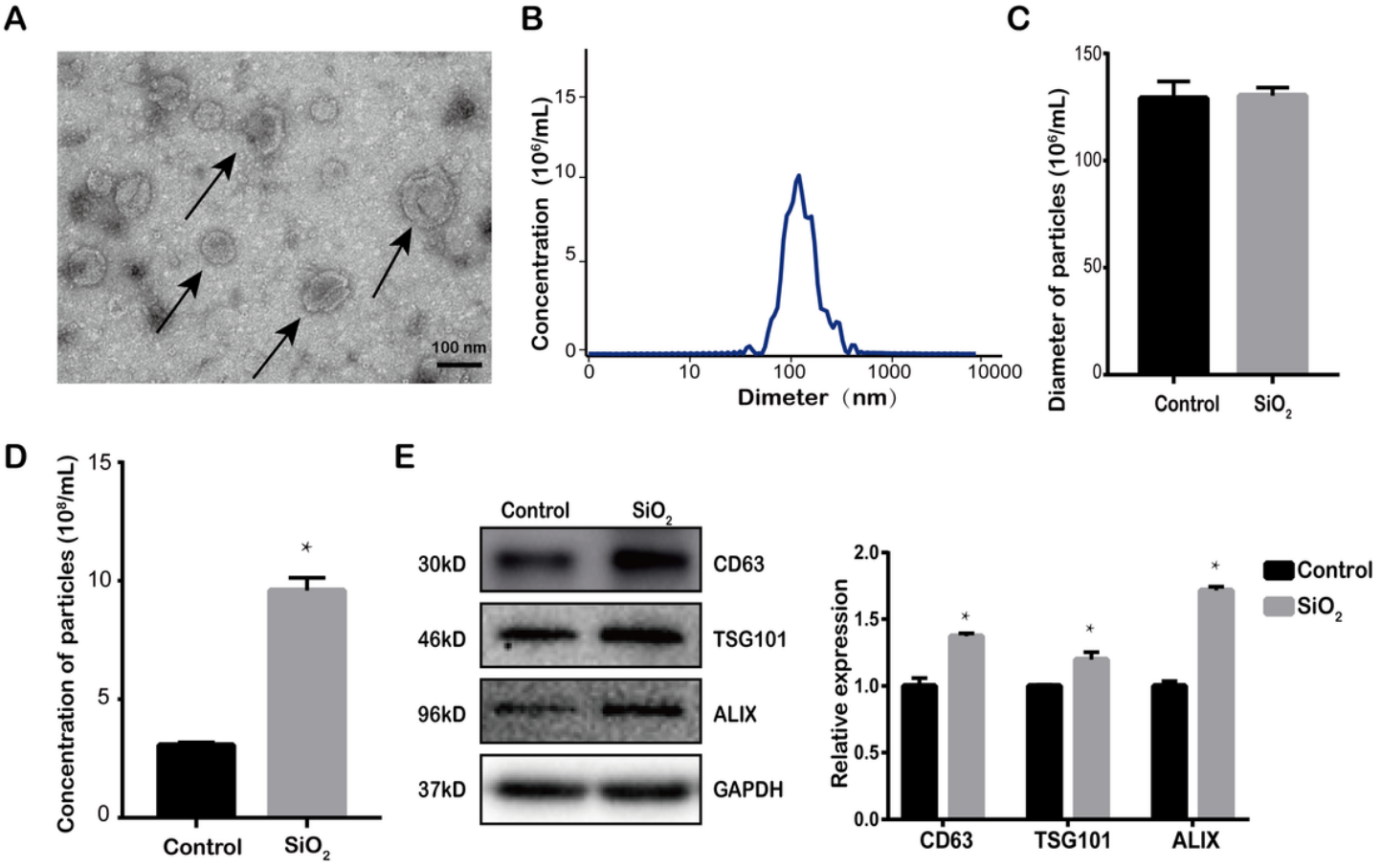

Figure 4

Characterization of exosomes derived from cell supernatant of macrophages. Morphology of the exosomes under a transmission electron microscope (a). Exosomes, a cup-shaped like, were indicated by black arrows. Scale bar, 100 nm. The diameter distribution and concentration of the particles (b). Histogram of the particles diameter (c) and the particles concentration (d). The expression of ALIX,

TSG101 and CD63 analyzed by Western blot (e). Control, macrophages exposed to PBS; SiO2, macrophages exposed to silica particles. The experiment were performed three times. Error bars indicate mean ± standard deviation. *Control vs. SiO2, P<0.05.

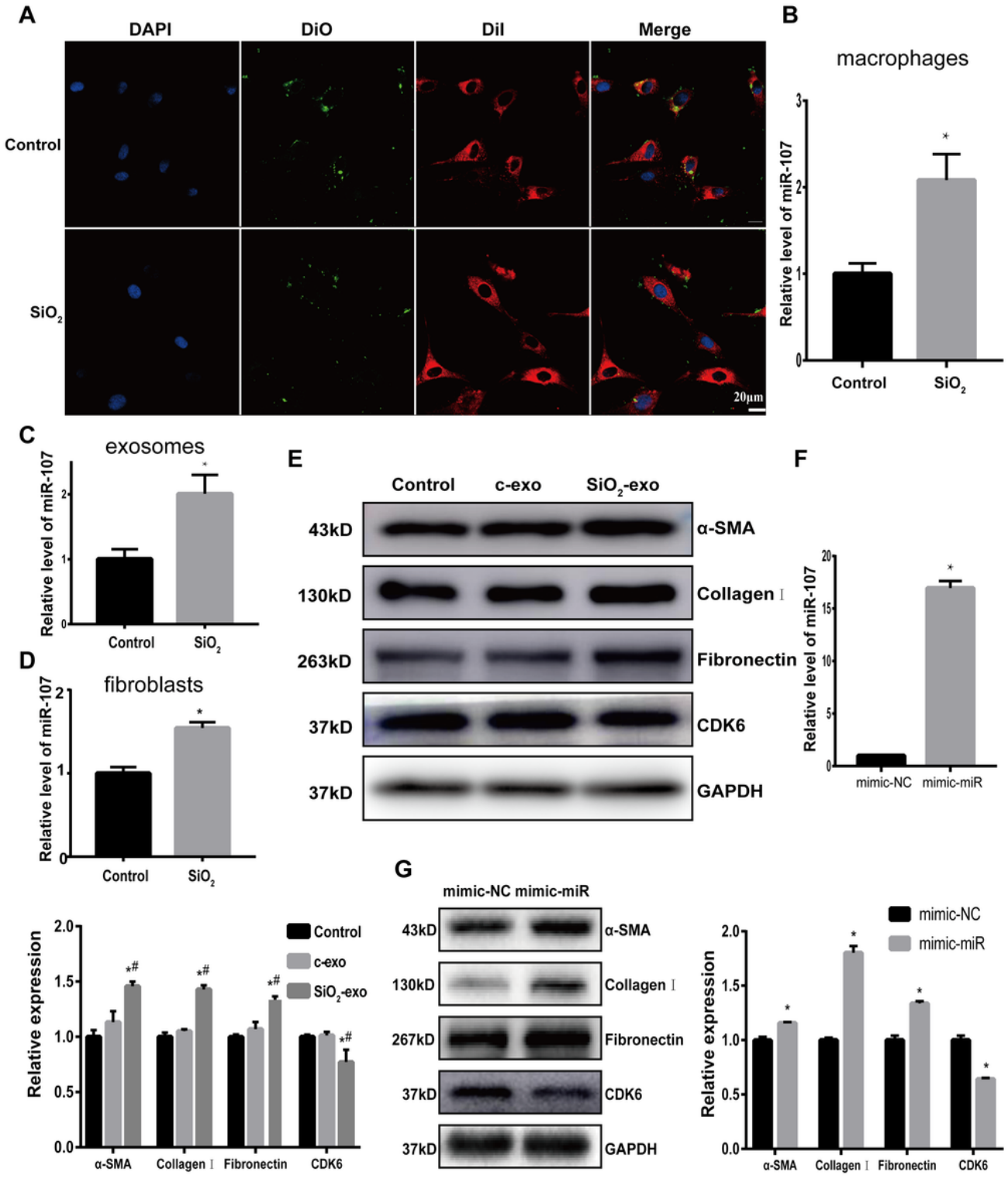

Figure 5

Role of exosomes derived from macrophages in fibroblasts transdifferentiation. The uptake of exosomes captured by a laser scanning confocal microscope (a). ¬¬Green (DiO), exosomes; red (DiI), NIH-3T3 cells;

blue (DAPI), nuclei. Relative levels of miR-107 of macrophages (b). Control, macrophages exposed to PBS; SiO2, macrophages exposed to silica particles. *P<0.05. Relative levels of miR-107 of exosomes (c). Control, exosomes derived from macrophages exposed to PBS; SiO2, exosomes derived from macrophages exposed to silica particles. *P<0.05. Relative levels of miR-107 of NIH-3T3 cells (d). Control, NIH-3T3 cells incubated with exosomes derived from macrophages exposed to PBS; SiO2, NIH-3T3 cells incubated with exosomes derived from macrophages exposed to silica particles. *P<0.05. The expression of fibrosis markers and CDK6 analyzed by Western blot (e). Control, NIH-3T3 cells exposed to PBS; c-exo, NIH-3T3 cells incubated with exosomes derived from macrophages exposed to PBS; SiO2-exo, NIH-3T3 cells incubated with exosomes derived from macrophages exposed to silica particles. *compared to control, P<0.05; #compared to c-exo, P<0.05. Relative levels of miR-107 of macrophages transfected with miR-107 mimic or negative control (f). The expression of relative proteins of macrophages transfected with miR-107 mimic or negative control (g). mimic-NC, NIH-3T3 cells incubated with exosomes derived from macrophages which transfected with negative control; mimic-miR, NIH-3T3 cells incubated with exosomes derived from macrophages which transfected with miR-107 mimic.* mimic-NC vs. mimic-miR, P<0.05. The level of miR-107 was normalized by U6 and the expression of relative proteins was normalized by GAPDH. The experiment were performed three times. Error bars indicate mean ± standard deviation. The levels of miR-107 were normalized by U6 and the expression of relative proteins was normalized by GAPDH.

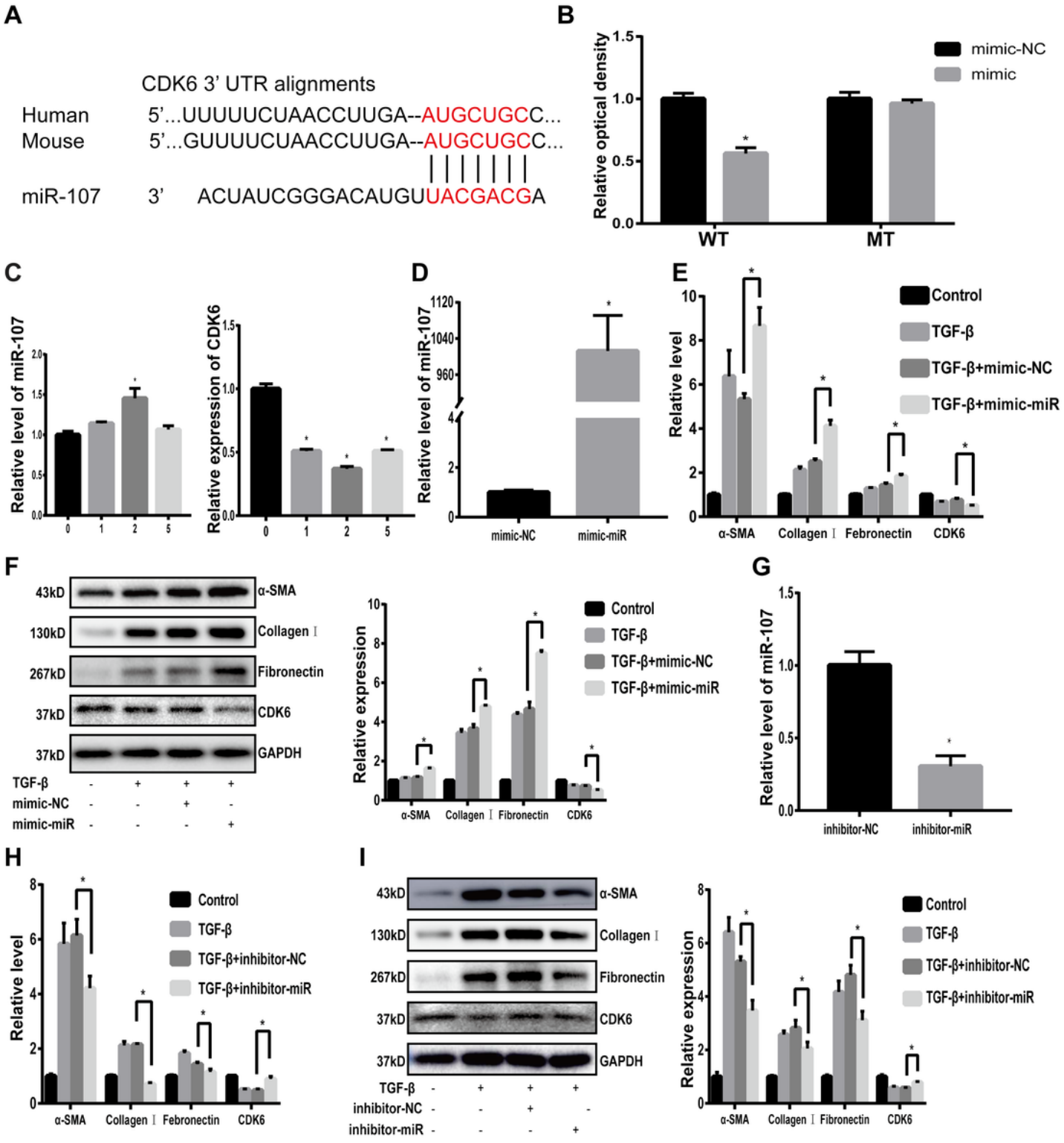

Figure 6

Role of miR-107 in fibroblasts transdifferentiation. Sketch map of predicted binding sites for miR-107 in 3'UTR of CDK6 (a). Seed sequence was labeled in red color. Validation of the target between miR-107 and CDK6 analyzed by dual luciferase reporter (b). *P<0.05. Relative levels of miR-107 and CDK6 in NIH-3T3 cells treated with different dose of TGF-β (0,1,2,5 ng/mL) (c). *compared to 0, P<0.05. Relative levels of miR-107 in NIH-3T3 cells transfected with miR-107 mimic or negative control (d). *P<0.05. The mRNA

levels of fibrosis markers and CDK6 in NIH-3T3 cells transfected with miR-107 inhibitor or negative control (e). *TGF-β+mimic-NC vs. TGF-β+mimic-miR, $P<0.05$. The expression of relative proteins (f). *TGF-β+mimic-NC vs. TGF-β+mimic-miR, $P<0.05$. Relative levels of miR-107 in NIH-3T3 cells transfected with miR-107 inhibitor or negative control (g). The mRNA levels of fibrosis markers and CDK6 in NIH-3T3 cells transfected with miR-107 inhibitor or negative control (h). *TGF-β+inhibitor-NC vs. TGF-β+inhibitor-miR, $P<0.05$. The expression of relative proteins in NIH-3T3 cells transfected with miR-107 inhibitor or negative control (i). *TGF-β+inhibitor-NC vs. TGF-β+inhibitor-miR, $P<0.05$. The experiment were performed three times. Error bars indicate mean ± standard deviation. The level of miR-107 was normalized by U6 and the protein/mRNA level of relative genes was normalized by GAPDH.

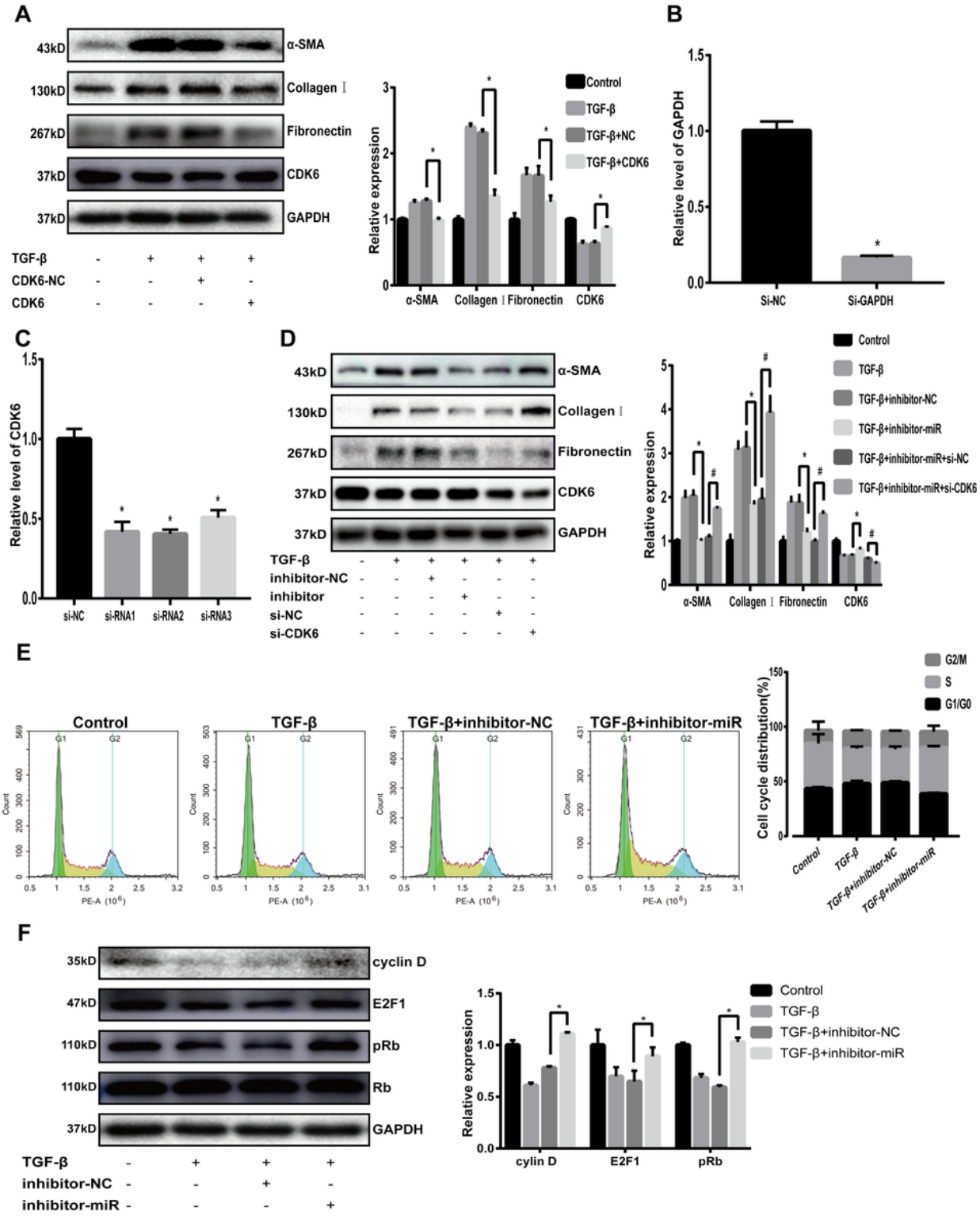

Figure 7

miR-107 promote fibroblasts (NIH-3T3 cells) transdifferentiation by targeting CDK6 through the cell cycle signaling pathway. The expression of fibrosis markers and CDK6 in NIH-3T3 cells transfected with CDK6 siRNA or negative control analyzed by Western blot (a). *TGF-β+NC vs. TGF-β+CDK6, P<0.05. The mRNA levels of GAPDH in NIH-3T3 cells transfected with GAPDH siRNA or negative control (b). *P<0.05. Knockdown efficiency of three siRNAs (c). *compared to si-NC, P<0.05. The expression of fibrosis markers

and CDK6 in NIH-3T3 cells in cell recovery experiment (d). *TGF-β+inhibitor-miR+si-NC vs. TGF-β+inhibitor-miR+si-CDK6, P<0.05. The cell cycle of the NIH-3T3 cells transfected with 2ng/mL TGF-β and miR-107 inhibitor or negative control (e). *TGF-β+inhibitor-NC vs. TGF-β+inhibitor-miR, P<0.05. The expression of proteins downstream of CDK6 in the cell cycle signaling pathway (f). *TGF-β+inhibitor-NC vs. TGF-β+inhibitor-miR, P<0.05. The experiment were performed three times. Error bars indicate mean ± standard deviation. GAPDH was used as an endogenous control.

Supplementary Files

This is a list of supplementary files associated with this preprint. Click to download.

- GraphicalAbstract.pdf
- SupplenmentaryMaterials.docx